KSCE Journal of Civil Engineering (2011) 15(4):707-719
DOI 10.1007/s12205-011-0011-9

*Energy Geotechnology*
www.springer.com/12205

# $CO_2$ Geological Storage − Geotechnical Implications

**D. N. Espinoza*, S. H. Kim**, and J. C. Santamarina*****

Received August 31, 2010/Accepted February 16, 2011

## Abstract

Fossil fuels account for more than 90% of the world total energy consumption. The emission of $CO_2$ to the atmosphere can be reduced by the development and implementation of carbon capture and storage technologies. The geological formations considered for $CO_2$ storage are saline aquifers, depleted and semidepleted hydrocarbon reservoirs, and unminable coal seams. The efficient short-term injection and the stable long-term geological storage of carbon dioxide are affected by complex hydro-chemo-mechanical interactions that take place in the formation, including water acidification, mineral dissolution, and stress and volume changes. Positive feedback mechanisms may lead to runaway effects. These hydro-chemo-mechanical coupled processes and emergent phenomena may hinder the storativity of injected carbon dioxide. Technological developments such as adequate geophysical tools for injection and reservoir monitoring, are needed for the safe geo-storage of $CO_2$.

Keywords: *carbon dioxide, sustainability, geological storage, reservoir engineering, geotechnical implication, leaks*

## 1. Introduction

Quality of life, in terms of education, infant mortality and life expectancy, correlates with energy consumption. Global energy consumption will increase dramatically in the next decades, and it will largely rely on fossil fuels because of the available reserves, their low cost, the investment in current infrastructure, and the still limited development of renewable energy. Currently, 90% of the total primary energy sources in the world are fossil fuels, and more than 85% in the USA (DOE, 2010).

The use of fossil fuels is intimately linked to the emission of $CO_2$ into the atmosphere. The current concentration of $CO_2$ in the atmosphere is ~385 ppm (parts per million), which is almost twice the concentration before the Industrial Revolution (200 ppm - IPCC, 2001). Anthropogenic $CO_2$ global emissions add to ~7 GtC/year (see Fig. 1). The USA releases 1.59 GtC/yr and China 1.78 GtC/yr – 2007 data (CDIAC, 2009). Power plants account for ~40% of total $CO_2$ emissions. Once released into the atmosphere, $CO_2$ enters into the global carbon cycle and interacts with the ocean and terrestrial sinks as shown in Fig. 2.

The estimated net annual increase of $CO_2$ concentration in the atmosphere is problematic since $CO_2$ is a greenhouse gas. The mean surface temperature has increased ~0.6±0.2°C since the industrial revolution, and atmospheric models forecast as much as a ~3°C increase by 2100 if anthropogenic $CO_2$ emissions continue current trends (Fig. 3). The UN Framework Convention on climate change has suggested that the atmospheric concentration of $CO_2$ should not exceed 450 ppm to prevent a major impact on climate conditions. Several technologies have been proposed for mitigating the emission of $CO_2$ into the atmosphere (Table 1). Two clear options call for reducing the combustion of fossil fuels, and capturing the generated $CO_2$ followed by permanent sequestration.

Suggested minimum storage time for $CO_2$ geological storage

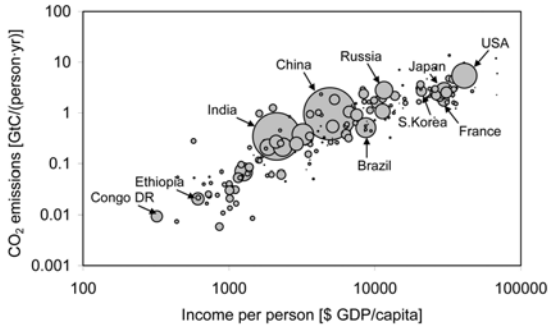


Fig. 1. Annual $CO_2$ Emissions per Person as a Function of Gross Domestic Product (adjusted for inflation) for Different Countries (Data from the Carbon Dioxide Information Analysis Center (www.cdiac.ornl.gov) and (www.gapminder.org).)

*Ph.D. Candidate, School of Civil and Environmental Engineering, Georgia Institute of Technology, Atlanta, GA 30332, USA (Corresponding Author, E-mail: nicolas@ce.gatech.edu)
**Ph.D. Candidate, School of Civil and Environmental Engineering, Georgia Institute of Technology, Atlanta, GA 30332, USA (E-mail: seunghee.kim@gatech.edu)
***Professor, School of Civil and Environmental Engineering, Georgia Institute of Technology, Atlanta, GA 30332, USA (E-mail: jcs@gatech.edu)

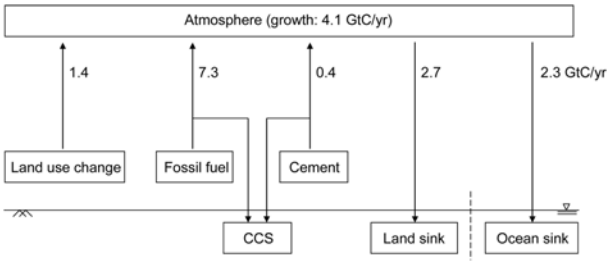


Fig. 2. Anthropogenic Perturbation of the Carbon Dioxide Cycle (Values show the annual contribution of various components (data from: Global-Carbon-Project 2010).)

ranges between 1,000 and 10,000 years. This requirement is less demanding than for nuclear waste in part due to the expectation that future technological developments might find other methods to mitigate global warming, and because of natural climate fluctuations such as the average glacial cycle period of 28,000 years (Augustin *et al*., 2004). Figure 4 shows a comparison of time scales for different processes related to human activities and geologic processes relevant to energy. The dramatic contrast

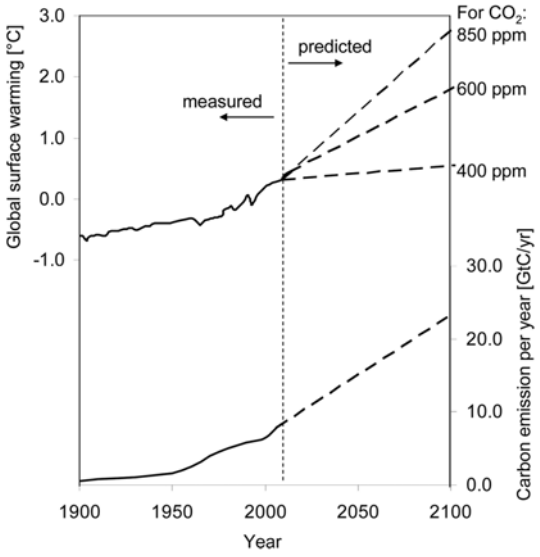


Fig. 3. Past and Extrapolated Future $CO_2$ Emissions (data from: Pacala and Socolow 2004; World-Resources-Institute 2010a) and Global Warming Predictions for Different $CO_2$ Levels (data from: Solomon, 2007)

Table 1. $CO_2$ Emission Mitigation Technologies

| $CO_2$ emission mitigation technology | Advantages | Difficulties | Capacity and certainty of execution |
|---|---|---|---|
| *DIRECT - capture, transport, and final sequestration of $CO_2$ generated from fossil fuel power plants* | | | |
| $CO_2$ geological storage coupled or not with fuel switching | - Available injection technology<br>- Large capacity<br>- May give additional revenue by enhanced hydrocarbon production | - Cost: it needs additional energy consumption ~20% for carbon capture and storage(1)<br>- Monitoring, contamination, and liability | - Large capacity: $10^3$~$10^4$ $GtCO_2$, mostly in saline aquifers(2) |
| Ocean storage | - Easy and relatively inexpensive<br>- No porous media involved | - Water acidification and effects on aquatic life(3)<br>- Transportation to the site | - Very large capacity >> $10^3$ $GtCO_2$ (volume of the ocean deeper than ~3000 m) |
| Chemical carbonation | - Thermodynamically stable | - Expensive and labor intensive | - Very limited; for example: annual production of concrete is ~15 Gt concrete |
| *INDIRECT - produce $CO_2$ - free energy, improve energy conservation and efficiency, or increase $CO_2$ natural uptake* | | | |
| *Alternative energy sources* | | | |
| Renewables, Solar, Wind, Geothermal | - Almost C-free | - Small contribution to the energy portfolio | - Currently provide 4% of the energy demand(4) |
| Nuclear fission | - Almost C-free<br>- Available technology | - Nuclear waste<br>- Non-commercial use of nuclear power technology | - Currently provide 6% of the energy demand(4) |
| Biofuels | - Consume bio-products in excess, e.g. sugar cane and corn | - Competes with food supply | - In Brazil ethanol accounts for less than 5% of the energy production(5) |
| *Conservation and efficiency* | | | |
| Change in people's habits - e.g. promote mass transit | - Almost no cost | - Requires time and policy | - Some countries are already highly efficient |
| More efficient end-use energy technologies and appliances - HVAC | - In progress | - It needs market-transforming policies(6) | - Efficient implementation could reduce carbon emissions from the building sector to levels equivalent to those 20 years ago |
| *$CO_2$ surface uptake* | | | |
| Terrestrial uptake | - Relatively inexpensive | - Difficult to increase natural sinks (trees, algae)<br>- Uncertainties about land use in the future(7) | - Currently at maximum<br>- Uptake about ~20% of total emissions |

(1) (Dooley *et al*., 2006; Heddle *et al*., 2003); (2) (IPCC, 2005); (3) (Golomb, 1993; House *et al*., 2006); (4) (IEA, 2009); (5) (World-Resources-Institute, 2010b); (6) (Brown and Southworth, 2008); (7) (Jaccard, 2005)

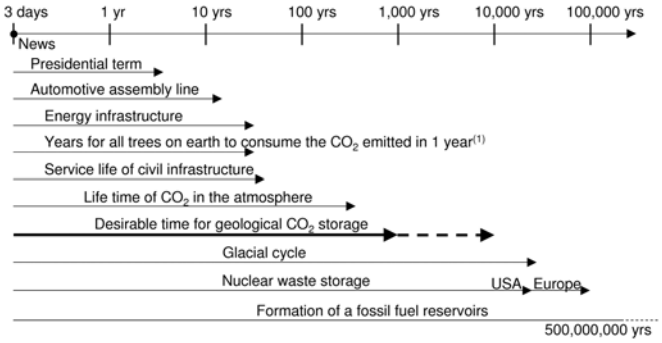


Fig. 4. Time Scales of Relevant Energy-Related Activities and Processes (Note: (1) Estimation based on the capacity of forest to absorb carbon in the atmosphere, 0.17 GtC/yr, from IPCC 2001).)

between political, engineering, and geological time scales add difficulty to short-time decision making.

The purpose of this manuscript is to explore geotechnical concepts relevant to carbon dioxide geological storage. First, we review the chemo-physical properties of water-$CO_2$-mineral systems, reservoir conditions, and the fundamentals of $CO_2$ geological storage. Next, we explore various hydro-chemo-mechanical coupled processes that may lead to emergent phenomena and increase the probability of geotechnical hazards. Finally, we investigate potential geophysical strategies to monitor the evolution of $CO_2$ storage projects.

## 2. $CO_2$ Geological Storage and Reservoir Conditions

### 2.1 Volume Estimation

The injected $CO_2$ displaces the original fluids that fill the voids in geological formations. The volume of the geological formation $V_{bulk}$ affected by the injection of a volume of $CO_2$ $V_{CO2}$ is a function of the average porosity of the reservoir $n$:

$$V_{bulk} = \frac{1}{\psi}\frac{V_{CO2}}{n} \quad (1)$$

where the displacement efficiency coefficient is $\psi \sim 0.6$ in media with spatially correlated random porosity and can be very low $\psi < 0.1$ if fingered invasion takes place (note: buoyancy effects, closed hydraulic boundary conditions, and the use of multiple injection wellbores can lower efficiency by as much as $\psi \sim 0.01$ (refer to Ehlig-Economides and Economides, 2010)). Let's assume a target sequestration of 4 GtC/year (for a flat trend based on present data – Fig. 3). The total amount of $CO_2$ to be sequestered in the next 50 years is 200 GtC or 730 $GtCO_2$. In a compressed state ($\rho_{CO2} \sim 0.7$ tonnes/m$^3$), this mass would occupy a volume $V_{CO2} = 1{,}050$ km$^3$. The geological volume for storage would be $V_{bulk} \sim 27{,}500$ km$^3$ for a porosity $n \sim 0.2$, and displacement efficiency $\psi = 0.5$. A 100 m thick reservoir would extend ~325 km in each direction.

### 2.2 $CO_2$ Trapping

The trapping mechanisms to keep $CO_2$ within deep geological formations rely on physical as well as chemical processes (Dooley *et al.*, 2006; IPCC, 2005; Jaccard, 2005). Physical trapping mechanisms include structural and stratigraphic trapping by cap rocks, hydrodynamic trapping by slow aquifer currents, and capillary trapping by interfacial forces. Chemical trapping mechanisms include dissolution of $CO_2$ in water, mineralization, $CO_2$ adsorption on coal and rich-organic shales, and $CO_2$ hydrate formation. Most trapping mechanisms and safe disposal conditions are found and favored at depth. We note that there are natural accumulations of $CO_2$ in the Earth's upper crust where $CO_2$ has been contained for geological times such as the Ladbroke Grove and Katnook Gas Fields in southeastern Australia (Watson *et al.*, 2004).

### 2.3 Geological Formations

Stable sedimentary basins facilitate $CO_2$ storage, particularly when they are near emission points. These basins are found in

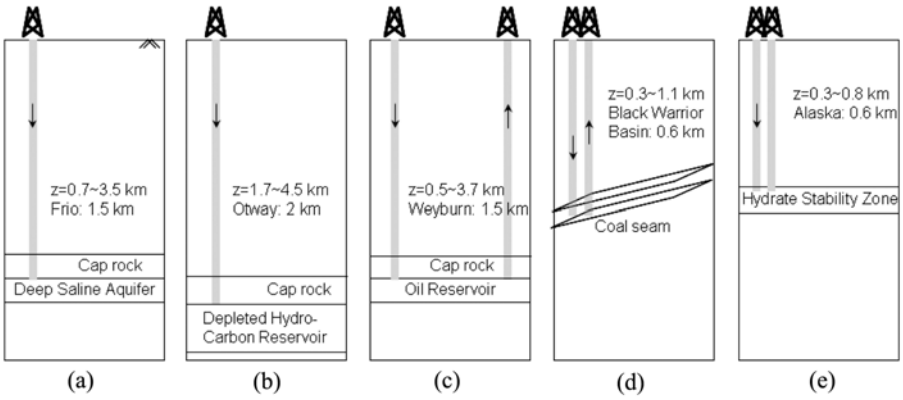


Fig. 5. $CO_2$ Storage Alternatives: (a) Deep Saline Aquifers, (b) Depleted Hydrocarbon Reservoirs, (c) $CO_2$-enhanced Oil Recovery, (d) $CO_2$-enhanced Gas Recovery from Coal Bed Methane, (e) $CO_2$-$CH_4$ Replacement in Hydrate Bearing Sediments (Depths shown for selected pilot projects.)

most continents (IPCC, 2005). The USA, Canada and Australia have extensive storage capacity (Dooley *et al*., 2006).

Favorable storage sites must have a thick accumulation of permeable sediments to maximize storage capacity and injectivity, overlain by a highly impermeable seal or cap rock (generally shale and evaporites).

The increase in effective stress with depth $z$ leads to low porosity fine grained sediment barriers. Pore size depends on porosity and specific surface. In high specific surface montmorillonitic shales, the mean poresize can be in the order of $10^{-8}$m (Armitage *et al*., 2010; Hildenbrand *et al*., 2002). High porefluid pressure at depth also lowers the mass density difference between water and $CO_2$, increases the solubility of $CO_2$ in water, and increases the adsorption of $CO_2$ in coal.

The geological system should be structurally simple. Candidate storage sites are assessed for reservoir size, depth and hydrogeology, geology and petrophysical characteristics of the reservoir and the seal cap rock, surface temperature and geothermal gradient, tectonic stability and faulting intensity, accessibility, infrastructure, and proximity to major $CO_2$ sources.

Figure 5 shows schematic diagrams of various formations for $CO_2$ geological storage. The principal targets for $CO_2$ injection are deep saline aquifers and depleted/semidepleted hydrocarbon reservoirs (which inherently include physical barriers and cap rocks). Injection into coal seams benefits from the co-production of $CH_4$. Similarly, hydrate-bearing sediments can also be used to sequester $CO_2$ while at the same time releasing $CH_4$ (a pilot test in the Alaska North Slope is planned for 2011, US DOE-NETL, project DE-NT0006553). Deep saline aquifers are most abundant and could store 110 to 2700 GtC (Gale, 2004).

### 2.4 Pilot Projects

There are more than 50 $CO_2$ injection projects reported worldwide (NETL, 2010). Figure 6 shows the mean pressure-temperature conditions at these storage sites. Most projects involve supercritical $CO_2$ and relatively small volumes.

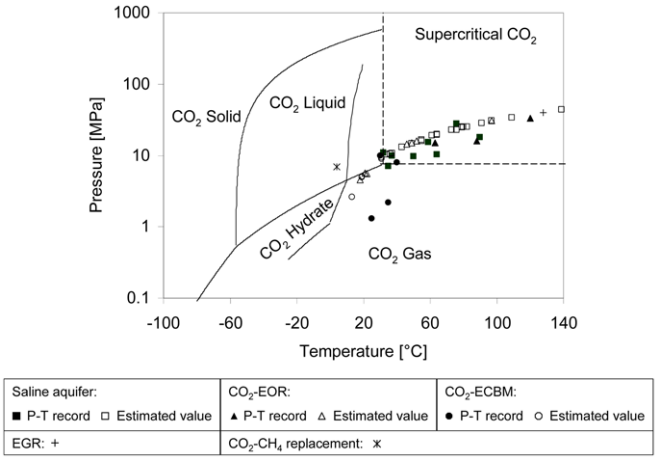


Fig. 6. Pressure-Temperature Dependent $CO_2$ Phases (Pilot $CO_2$ injection projects are superimposed on this plot. Unless reported in the original sources, the PT conditions are estimated as: $P = g\ \rho_w\ z$, $T = T_0$ (4°C) + 30°C/$km \cdot z$. ($CO_2$ hydrate phase boundary from Sloan and Koh 2008; Takenouchi and Kennedy, 1965).)

### 2.5 Implementation

The injection of $CO_2$ underground can be implemented with technology developed for petroleum and gas production. In fact, acid gas injection is routinely done in Alberta, $CO_2$-enhanced oil recovery is a common practice in oil reservoirs around the world, and there are more than ~5000 km of $CO_2$ pipelines in North America (Dooley *et al*., 2006). Still, the systematic geological storage of $CO_2$ will require improvements in risk assessment, adequate evaluation of regional capacity and reservoir integrity, matching emission sources with sinks, and enhanced monitoring technology (Gale, 2004). In addition to these technical difficulties, economical, political, and legal obstacles have hindered the adoption of CSS technologies.

## 3. Underlying Concepts and Implications

### 3.1 Geochemical Concepts

#### 3.1.1 Properties of $CO_2$

The combustion of fossil fuels yields $CO_2$ among other byproducts. For example, burning methane produces

$$CH_4 + 2\,O_2 \rightarrow CO_2 + 2\,H_2O \quad (2)$$

The physical properties of $CO_2$ depend on pressure-temperature P-T conditions. The $CO_2$ phase diagram is shown in Fig. 6. $CO_2$ is a gas at normal temperature and pressure, it turns into liquid at moderate pressures ~6.4 MPa at 298 K, and becomes supercritical when the temperature is higher than 304.1 K and the pressure is greater than 7.38 MPa. The mass density $\rho$ of $CO_2$ varies widely, in fact, $CO_2$ is heavier than seawater at pressures above ~28 MPa at 277.15 K ($\rho_{CO2}$=1035 kg/m$^3$). Mass density can be approximated with a cubic equation of state (Peng and Robinson, 1976) or using more accurate but complex equations (Span and Wagner,

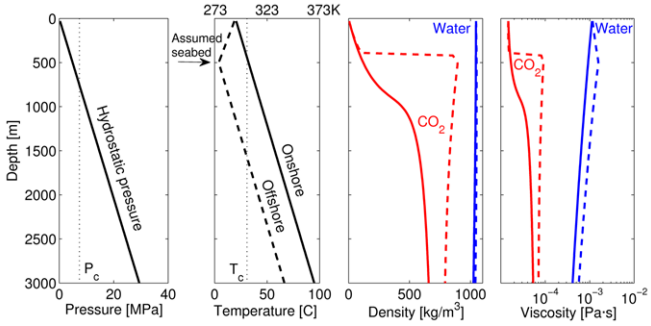


Fig. 7. Density and Viscosity of $CO_2$ and Water as a Function of Depth, Both on-Shore and Off-Shore (For an assumed seabed at 500 m, $P_c$ and $T_c$ are the critical pressure and temperature for $CO_2$. Note: the density of liquid $CO_2$ exceeds the density of deep seawater when the seabed is deeper than 3000 m.)

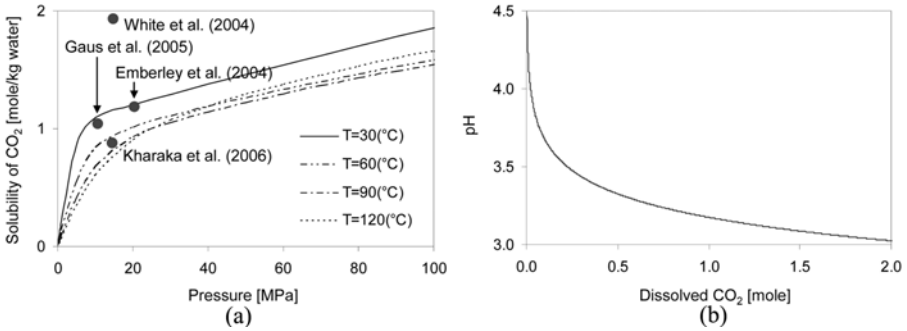


Fig. 8. $CO_2$ Solubility in Water and pH: (a) $CO_2$ Solubility in 1 m NaCl Aqueous Solution (Note: An increase in salinity reduces $CO_2$ solubility), (b) pH as a Function of Dissolved $CO_2$ (Note: Solubility data from Duan and Sun, 2003)

1996). The mass densities of water and $CO_2$ are plotted in Fig. 7 for typical P-T conditions present in onshore and offshore applications.

Other important P-T dependent properties of $CO_2$ include high bulk compressibility, typically an order of magnitude higher than that of water (Span and Wagner, 1996), and very low viscosity, typically 10 times lower than that of water as shown in Fig. 7, ($\mu_{CO2}$=$10^{-4}$ Pa·s at 10 MPa and 280 K - Fenghour *et al*., 1998).

### 3.1.2 Water-$CO_2$ Interaction and Properties

$CO_2$ dissolves in water to form aqueous carbon dioxide $CO_2$(aq). The solubility of $CO_2$ in water $x_{CO2}$ [mol/L] can be estimated using Henry's law

$$x_{CO2} = k_H \varphi P_{CO2} \quad (3)$$

where the Henry's coefficient is approximately $k_H \approx 10^{-1.46} = 0.0347$ and the fugacity coefficient $\varphi \leq 1$ can be estimated with an equation of state. Water at room temperature and at 0.1 MPa contains $x_{CO2} \approx$ 0.03-to-0.04 mol/L. That solubility increases by two orders of magnitude $x_{CO2} \approx$ 1-to-2 mol/L as pressure and temperature increase to reservoir conditions, i.e., one to two moles of $CO_2$ per liter of brine (Fig. 8).

Part of the aqueous carbon dioxide mixes with water to produce carbonic acid and ionizes stepwise:

$$\begin{aligned} &CO_2(g) \Leftrightarrow CO_2(aq) && \text{Henry's law} \quad (4)\\ &CO_2(aq) + H_2O(l) \Leftrightarrow H^+ + HCO_3^-(aq) && \log K_{eq} = -6.35,\\ &HCO_3^-(aq) \Leftrightarrow H^+ + CO_3^{2-}(aq) && \log K_{eq} = -10.33 \end{aligned}$$

The final result of adding $CO_2$ to water is the production of ion bicarbonates, an increase in $H^+$, and a decrease in pH. At reservoir conditions, $CO_2$ dissolution in water yields a pH ≈ 3 (Fig. 8).

Other relevant properties of the water-$CO_2$ system include (a) solubility of water in liquid and supercritical $CO_2$ (~0.05 mol of water per kg of liquid $CO_2$ at 10 MPa and 285 K - Spycher *et al*., 2003), (b) high diffusivity of water into liquid $CO_2$ (D ≈ 2-to-20×$10^{-8}$m$^2$/s - at 7-25 MPa and 305±10 K - Espinoza and Santamarina, 2010), and (c) $CO_2$ hydrate formation at high pressure and low temperature (Fig. 6; Sloan and Koh, 2008).

Table 2. Mineral Reactions with $CO_2$-Acidified Water

| Mineral | Typical reaction | Reaction rate | Notes |
|---|---|---|---|
| 1) Silicates[a)] | $SiO_{2(s)} + 2H_2O \Leftrightarrow H_4SiO_4$ $\Leftrightarrow H^+ + H_3SiO_4^-$ $\Leftrightarrow H^+ + H_2SiO_4^{2-}$ | $1.26\times10^{-14}$ mol·m$^{-2}$s$^{-1}$ (White *et al*., 2005) | · Solubility of quartz does not change with concentration of dissolved $CO_2$ |
| 2) Aluminosilicates[b)] | Anorthite: $CaAl_2Si_2O_{8(s)} + 8H^+ \Leftrightarrow Ca^{2+} + 2Al^{3+} + 2H_4SiO_4$, $K_{eq} = 10^{21.7}$<br>Kaolinite: $Al_2Si_2O_5(OH)_4(s) + 6H^+ \Leftrightarrow 2Al^{3+} + 2H_4SiO_4 + H_2O$, $K_{eq} = 10^{3.8}$ | Anorthite: $1.2\times10^{-5}$ mol·m$^{-2}$s$^{-1}$<br>Oligiocalse: $1.2\times10^{-8}$ mol·m$^{-2}$s$^{-1}$<br>Albite: $3.6\times10^{-9}$ mol·m$^{-2}$s$^{-1}$<br>Kaolinite: $10^{-14}$-to-$10^{-15}$ mol·m$^{-2}$s$^{-1}$<br>(Gaus *et al*., 2005) | · Include feldspars, micas, and clays.<br>· Reaction rate is slow.<br>· Yields more dissolved cations than carbonate.<br>· Results in pH up to 8. |
| 3) Carbonates[c)] | $CaCO_{3(s)} + H^+ \Leftrightarrow Ca^{2+} + HCO_3^-$, $K_{eq} = 10^{1.85}$<br>$CaCO_{3(s)} + CO_2 + H_2O \Leftrightarrow Ca^{2+} + 2HCO_3^-$, $K_{eq} = 10^{-4.5}$<br>$CaCO_{3(s)} + H_2O \Leftrightarrow Ca^{2+} + HCO_3^- + OH^-$, $K_{eq} = 10^{-8.48}$ | Calcite: $1.6\text{-to-}3.2\times10^{-5}$ mol·m$^{-2}$s$^{-1}$ (Brosse *et al*., 2005) | · Faster than aluminosilicates<br>· Solubility depends on T, P, Salinity, ionic concentration, and pH<br>· Dissolution rate is fast, but overall amount of reaction is small<br>· Results in pH from 3 to 5 |

Sources: (a) (Drever, 1997); (b) (Li *et al*., 2006); (c) (Algive *et al*., 2009; Fredd and Fogler, 1998; Renard *et al*., 2005; Stumm and Morgan, 1996)

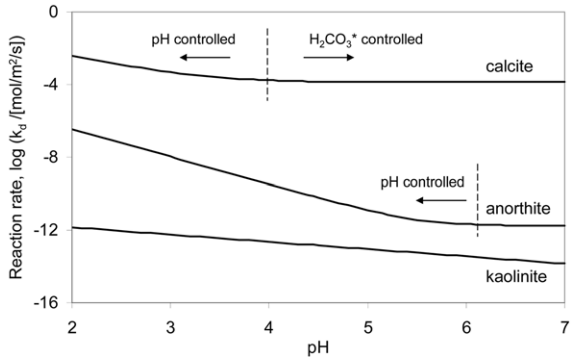


Fig. 9. Reaction Rate log ($k_d$ / [mol/m$^2$/s]) for Calcite $CaCO_3$, Anorthite $CaAl_2Si_2O_8$, and Kaolinite $Al_2Si_2O_5(OH)_4$ at a Temperature of 40°C and $[CO_{2(aq)}]$ = 1 mole (For calcite, $k_d = k_1[H^+] + k_2[H_2CO_3^*]$ where $k_1 = 0.745$, $k_2 = 8.6\text{x}10^{-4}$ [mol/m$^2$/s] at 40°C (Algive *et al*., 2009; Fredd and Fogler, 1998; Pokrovsky *et al*., 2005; Renard *et al*., 2005). For anorthite, $k_d = k_H[H+]^{1.5} + k_{H2O} + k_{OH}[OH^-]^{0.33}$ where $k_H = 6.883\text{x}10^{-4}$, $k_{H2O} = 3.58\text{x}10^{-12}$, and $k_{OH} = 4.51\text{x}10^{-14}$ [mol/m$^2$/s] at 40°C (Li *et al*., 2006). For kaolinite, $k_d = k_H[H+]^{0.4} + k_{OH}[OH^-]^{0.3}$ where $k_H = 2.79\text{x}10^{-11}$ and $k_{OH} = 3.51\text{x}10^{-16}$ [mol/m$^2$/s] at 40°C (Li *et al*., 2006).)

### 3.1.3 Water-$CO_2$-Mineral Interaction

Table 2 summarizes representative chemical reactions, typical reaction rates and related comments. The equilibrium constant for dissolution reaction denotes the concentration of produced species relative to the concentration of reactant species at steady state conditions, i.e., a function of mineral solubility. The solubility of minerals in water depends on pH. (Stumm and Morgan, 1996). Furthermore, the reaction rate of minerals in $CO_2$-water depends on temperature, pressure (i.e., $CO_2$ solubility and pH), and the concentration of other species (Algive *et al*., 2009; Fredd and Fogler, 1998; Pokrovsky *et al*., 2005; Renard *et al*., 2005). Dissolution rates for calcite $CaCO_3$, anorthite $CaAl_2Si_2O_8$, and kaolinite $Al_2Si_2O_5(OH)_4$ are plotted as a function of pH in Fig. 9. Silicates yield more dissolved cations (pH up to 8) than carbonates (pH up to 5) but the reaction rate is much slower (Gunter *et al*., 2000). Consider 1 mm spheres of calcite, anorthite, and kaolinite submerged into water acidified by 1 mole of dissolved $CO_2$ per liter (pH~3). Using dissolution rates in Fig. 9 and assuming that the system is far from equilibrium, the time required to dissolve each sphere is 4 hours for calcite, 16 years for anorthite, and 226 years for kaolinite. It is also important to recognize the high reactivity of water dissolved in $CO_2$ with steel and minerals (McGrail *et al*., 2009).

### 3.1.4 $CO_2$ Adsorption on Organic Surfaces

Coal and organic shales adsorb $CO_2$ (DOE-NETL, 2008; Larsen, 2004). Langmuir-type sorption isotherms are commonly used to characterize the kinetics of the reaction at pressures < 10 MPa (Ceglarska-Stefanska and Zarebska, 2002b; Mazumder, *et al*., 2006). For reference, about ~1.6 moles of $CO_2$ can be adsorbed per kg of coal at 3 MPa and 298 K (37 cm$^3$ of gas $CO_2$ at normal pressure and temperature per gram of coal). A higher fluid pressure promotes higher and faster uptake.

### 3.1.5 Summary

High fluid pressure and temperature bring $CO_2$ into liquid or supercritical phases and promote $CO_2$ solubility in water and adsorption onto organic surfaces. In the presence of $CO_2$, water acidifies and more intense and faster mineral dissolution takes place. Liquid and supercritical $CO_2$ exhibit much lower viscosity than water.

## 3.2 Mixed Fluid Conditions

### 3.2.1 Pressure Dependent $T_s$ and $\theta$

The water-$CO_2$ interfacial tension decreases from $T_s$~72 to 25 mN/m as the pressure increases from 0.1 MPa to 6.4 MPa at ~298 K, eventually $T_s$ reaches a plateau at $T_s \approx 25\pm5$ mN/m in the supercritical state (Espinoza and Santamarina, 2010; Kvamme *et al*., 2007). Furthermore, the contact angle formed by the $CO_2$-water interface on mineral surfaces varies with fluid pressure in response to changes in $CO_2$-water interfacial tension: as the fluid pressure increases, the contact angle increases on non-wetting surfaces such as oil-wet quartz and coal and slightly decreases in water-wet quartz and calcite surfaces (Chalbaud *et al*., 2009; Chi *et al*., 1988; Chiquet *et al*., 2007; Dickson *et al*., 2006; Espinoza and Santamarina, 2010).

Changes in interfacial tension $T_s$ and contact angle $\theta$ will affect the capillary pressure, the evolution of flooding, the residual saturation, relative permeabilities, and capillary effects. In its simplest form, capillary pressure $\Delta P_c$ [Pa] is estimated from Laplace's equation:

$$\Delta P_c = P_{CO2} - P_w = \frac{2T_s}{r}\cos\theta \tag{5}$$

### 3.2.2 Breakthrough Pressure

The breakthrough pressure $P^*_{thru}$ when $CO_2$ percolates through a porous medium depends on the mean pore size expressed in terms of specific surface $S_s$ and void ratio $e = e_{1kPa} - C_c \log(p'/1\text{ kPa})$, the wettability of the minerals in the presence of water and $CO_2$, and the standard deviation in pore size distribution. We can extend Laplace's capillary pressure equation to obtain the following expression for the breakthrough pressure (Espinoza and Santamarina, 2010):

$$P^*_{thru} = \psi \frac{S_s \rho T_s \cos\theta}{e_{1\text{kPa}} - C_c \log\dfrac{p'}{1\text{kPa}}} \tag{6}$$

where $p'$ is the in situ effective stress, and the factor $\psi$ depends on clay fabric and grain size distribution; a value of $0.04<\psi<0.08$ applies to smectite clay barriers. The sealing capacity of cap rocks will depend on this breakthrough pressure; thereafter, the leak rate will be determined by the cap rock permeability to $CO_2$ (Fleury *et al*., 2010; Pusch *et al*., 2010).

### 3.2.3 Differences in Mass Density - Convection and Self Mixing

$CO_2$ is lighter than water or brine at reservoir P-T conditions (Fig. 7). The Bond number $B$ quantifies gravity-driven $CO_2$ migration as a function of the mass density difference ($\rho_w - \rho_{CO2}$) relative to capillary forces $T_s \cdot \cos\theta$ (Pennell *et al*., 1996):

$$B = \frac{(\rho_w - \rho_{CO_2}) g k k_{rCO2}}{T_s \cos\theta} \quad (7)$$

The mass density of the water with $CO_2$ in solution $\rho_{sol}$ [kg/m$^3$] is slightly heavier than the formation water and can be estimated from the mass density of pure water $\rho_w$ [kg/m$^3$] and the concentration of $CO_2$ in water $x_{CO2}$ [mol/m$^3$] as:

$$\rho_{sol} = \rho_w + m_{CO2} x_{CO2} - x_{CO2} \rho_w V_\varphi \quad (8)$$

where $m_{CO2}$[kg/mol] is the molecular weight of $CO_2$, and $V_\varphi$ [m$^3$/mol] is the apparent molar volume of dissolved $CO_2$ as a function of temperature T[C], $V_\varphi = 37.51 \cdot 10^{-6} - 9.585 \cdot 10^{-8}\ T + 8.740 \cdot 10^{-10}\ T^2 - 5.044 \cdot 10^{-13}\ T^3$ (Garcia, 2001). For example, there is an increase in density $\Delta\rho \sim 10$ kg/m$^3$, for water saturated with $CO_2$ at 10 MPa and 313K ($x_{CO2} \sim 1230$ mol/m$^3$). Dissolution-densification and gravity-driven flow will cause convective transport which will accelerate $CO_2$ mixing in the reservoir water (Kneafsey and Pruess, 2010; Riaz *et al*., 2006).

### 3.2.4 Differences in Viscosity: Fingering

Two dimensionless numbers control the pattern of fluid displacement: (1) the ratio of viscosities $M$ between the invading fluid $\mu_{CO2}$ and the displaced fluid $\mu_w$, and (2) the capillary number $C$ which is the ratio between viscous and capillary forces:

$$M = \frac{\mu_{CO2}}{\mu_w} \quad (9)$$

$$C = \frac{q \mu_{CO2}}{T_s \cos\theta} \quad (10)$$

where $q$[m$^3$/s/m$^2$] is the injection rate, $T_s$[N/m] is the interfacial tension between water and $CO_2$, and $\theta$ is the contact angle formed by the water-$CO_2$ interface and the mineral surface. Stable displacement takes place when $M > 1$ and $C > 1$, viscous fingering when $M << 1$, and capillary fingering when $C << 1$ (Lenormand *et al*., 1988). Since the viscosity of $CO_2$ is at least one order of magnitude lower than that of water at reservoir P-T conditions (Fig. 7), $CO_2$ may displace water from the pore space in the form of viscous fingers; in this case, the bulk volume of sediment $V_{bulk}$ involved in storage will increase dramatically (Eq (1)).

### 3.2.5 $CO_2$ Lowers the Viscosity of Oil

$CO_2$ dissolves in crude oil (typically alkanes with less than 13 carbon atoms at reservoir conditions with $P > 10$ MPa and $T > 320$ K), lowers the viscosity of the crude oil, and favors oil recovery (Blunt *et al*., 1993).

### 3.2.6 Summary

Interfacial tension and the capillary entry pressure for $CO_2$ into a water saturated seal cap rock decrease with pressure. The dissolution of $CO_2$ in water increases the density of water, promote gravity-driven flow and accelerate mixing. Pronounced differences in viscosity between liquid or supercritical $CO_2$ and water tend to promote viscous fingering during $CO_2$ injection.

## 3.3 Chemo-Hydro-Mechanical Coupling

### 3.3.1 Increased Fluid Pressure and Fault Reactivation

The increase in porefluid pressure during $CO_2$ injection can reactivate nearby faults if the state of effective stress approaches failure conditions (Rutqvist and Tsang, 2002; Streit and Hillis, 2004).

### 3.3.2 Capillary-Driven Deformation

The invasion of immiscible $CO_2$ in a water saturated reservoir gives rise to capillary forces and can cause significant volumetric deformation in fine-grained sediments (Delage *et al*., 1996).

### 3.3.3 Fluid-Driven Fracture Formation

Hydraulic fracture can take place in both cohesive-cemented and cohesionless-frictional sediments (Bjerrum *et al*., 1972; Jaworski *et al*., 1981; Zhai and Sharma, 2005). Particle-scale mechanisms compatible with the effective-stress dependent strength of sediments take into consideration capillary forces induced by the tensile membrane between $CO_2$ and water, seepage drag forces, and skeletal forces to explain particle displacement and localization (Shin and Santamarina, 2010).

### 3.3.4 Effects of pH and Permittivity on Interparticle Electrical Forces - Changes in Clay Fabric

Two fluid-mineral interactions anticipate changes in interparticle forces after $CO_2$ injection: (1) water acidification changes the mineral surface charge, and (2) the low permittivity of $CO_2$ ($\kappa' \sim 2$ to 3) compared to water ($\kappa' = 80$) implies changes in van der Waal's attraction (Israelachvili, 1991; Obriot *et al*., 1993; Palomino and Santamarina, 2005). These fluid-mineral phenomena will alter the equilibrium between van der Waal's attraction and double layer repulsion forces at the clay particle scale, cause changes in clay fabric, and affect the seal capacity of cap rocks.

### 3.3.5 Reactive Fluid Transport - Wormholes

Acidified water dissolves minerals and enlarges pores along transport channels (Emberley *et al*., 2004; Kaszuba *et al*., 2005; Watson *et al*., 2004). The hydraulic conductivity may increase by a factor of 10-to-100 (Verdon and Woods, 2007), with even small changes in global porosity, as can be predicted using the Kozeny-Carman model. Two dimensionless numbers control the evolution of dissolution patterns: Damköhler number represents the ratio between advection and reaction times $Da = \kappa l / v$ (reaction rate

$\kappa$[1/s], characteristic length $l$[m], velocity $v$[m/s]), while the Peclet number is the ratio between advection and diffusion time $Pe=vl/D$ (diffusion coefficient $D$[m$^2$/s]). The process is mass-transfer limited if a chemical reaction is very fast compared to mass-transfer kinetics $Da>>1$ (e.g., more likely in the dissolution of carbonates). Otherwise, the process is reaction-rate limited $Da<<1$ (e.g., more likely if the dissolution of aluminosilicates is involved). The dissolution pattern during reactive transport can be categorized as face/global dissolution ($Da>10^{-3}$, $Pe<10^{-3}$), dominant wormholes ($Da>10^{-3}$, $Pe>10^{-2}$), or uniform dissolution ($Da<10^{-3}$) (Golfier *et al*., 2002). A rapid mineral dissolution rate combines with the inherent sediment heterogeneity to facilitate a dominant wormholes tendency (Fredd and Fogler, 1998). Wormhole formation would lead to marked $CO_2$ leakage.

#### 3.3.6 Dissolution - Horizontal Effective Stress $k_0$ - Shear and Tensile Fractures

Complementary analytical, numerical (DEM and FEM), and experimental techniques show the effects of mineral dissolution and ensuing particle-level volume contraction on the evolution of the state of stress under constant overburden at zero-lateral strain boundary conditions during mineral dissolution. In particular, the stress ratio at zero lateral strain $k_0=\sigma'_h / \sigma'_v$ (Jaky, 1944; Mayne and Kulhawy, 1982) experiences a pronounced decrease during mineral dissolution, and it may reach the Rankine active failure condition $k_a$ on the Coulomb failure plane (Shin and Santamarina, 2009). Strain localization along shear planes may follow (Shin *et al*., 2008). Furthermore, mineral dissolution causes sediment compaction, and the cap rock may experience bending and tensile failure.

Table 3. Coupling and Emergent Phenomena

| Coupling | Emergent phenomenon |
|---|---|
| Multiphase fluid phenomena | - Relative hydraulic conductivities<br>- Differences in mass density and buoyancy<br>- Differences in viscosity and viscous fingering<br>- Fluid segregation<br>- Pressure dependent interfacial tension and contact angle<br>- Percolation and breakthrough pressure |
| Chemo-Hydro | - Reduction of oil viscosity by $CO_2$<br>- Dissolution followed by increased porosity and pore size<br>- Reactive transport and wormhole formation<br>- Spatial changes in hydraulic conductivity<br>- Gravity-driven self mixing, $CO_2$ diffusion, pendular water, mineral precipitation<br>- Coal $CO_2$ adsorption: reduced fluid conductivity and swelling pressure<br>- Hydrate formation and depressurization: fluid volume expansion, possible gas-driven fractures |
| Hydro-Mechanical | - Increased fluid pressure and lower effective stress<br>- Fault reactivation; hydraulic fracture of the cap rock<br>- Capillarity-driven contraction<br>- Fluid-driven fracture formation |
| Chemo-Mechanical | - pH and permittivity effects on DLVO, changes in clay fabric<br>- Pressure solution/precipitation<br>- Mineral dissolution and sediment compaction<br>- Cap rock bending failure<br>- Decrease in horizontal effective stress $k_0$ Shear fractures in contraction |
| Chemo-Hydro-Mechanical | - Combination of previous phenomena |

#### 3.3.7 Coal Swelling Pressure

Coal swells, its fluid conductivity decreases, and the effective stress increases with the adsorption of $CO_2$ (Mazumder *et al*., 2006; Pekot and Reeves, 2002; Somerton *et al*., 1975). Eventually, $CO_2$-$CH_4$ replacement in coal may become self-limiting because of coal swelling and reduced fracture porosity (Ceglarska-Stefanska and Zarebska, 2002a).

#### 3.3.8 Summary

The trapping mechanisms of $CO_2$ in geological formations rely on physical, chemical, and mechanical processes identified above. Each has different time and spatial scales. We summarize potential implications on $CO_2$ storage in Table 3.

## 4. Monitoring Strategies and Risk Assessment

$CO_2$ leakage from storage sites back into the atmosphere decreases the efficiency of $CO_2$ storage, may pollute drinking water aquifers and endanger living organisms. Faults and abandoned wells are preferential flow paths that add to the slow transport and diffusion through otherwise continuous strata (Dooley *et al*., 2006; Leuning *et al*., 2008). Monitoring is required to assess the movement of $CO_2$ and to detect leaks. The design of a monitoring strategy must consider the large areal extent of $CO_2$ storage reservoirs (on the order of ~km$^2$) and account for spatial and temporal variability.

Potential monitoring methods, most of them already available for other applications, are summarized in Table 4. These monitoring methods take advantage of differences between physical properties (mass density, bulk stiffness, electrical resistivity and dielectric permittivity, and thermal characteristics), the detection of byproducts from chemical reactions, or coupled process effects such as subsidence or micro-seismicity. Tracers such as $\delta^{13}$C and $SF_6$ may be included in the injected $CO_2$ to facilitate detection (Leuning *et al*., 2008). The most common subsurface geophysical methods for deep reservoir applications are based on elastic wave propagation and electrical resistivity (Kiessling *et al*., 2010; Nakatsuka *et al*., 2010). The following analysis expresses their applicability to $CO_2$ geological storage. The bulk modulus $B_{mix}$ of the sediment can be estimated from the Biot-Gassman equation:

$$B_{mix} = B_{sk}+\left(1-\frac{B_{sk}}{B_g}\right)^2\left[n\left(\frac{S_w}{B_w}+\frac{S_{CO2}}{B_{CO2}}\right)+\frac{1-n}{B_g}-\frac{B_{sk}}{B_g^2}\right]^{-1} \quad (11)$$

where subindices represent the skeleton *sk*, the mineral that makes the grains *g*, the water *w*, and the $CO_2$. The density of the mixture is:

Table 4. $CO_2$ Monitoring Techniques

| Method | Property measured | Principle, comments and issues |
|---|---|---|
| *1. SUBSURFACE MONITORING* | | |
| Porewater geochemistry[1] | $CO_2$, $HCO_3^-$, $CO_3^{2-}$, DIC, major ions, pH, alkalinity, salinity, and isotopes | $CO_2$ dissolves in water and changes water geochemistry |
| Seismic techniques[2] | P-wave velocity and amplitude | The bulk modulus of $CO_2$ is one order of magnitude lower than that of water |
| Electromagnetic techniques [3] | Resistivity and electromagnetic waves | High impedance mismatch of electrical conductivity and dielectric permittivity between $CO_2$ and formation water. |
| Temperature signal[4] | Temperature | $CO_2$ causes non-isothermal events such as expansion induced cooling of $CO_2$ and thermal heat dissipation from $CO_2$ dissolution |
| Infrared monitoring[5] | Infrared absorption | $CO_2$ gas shows characteristic absorption spectrum for infrared waves. |
| *2. NEAR SURFACE MONITORING* | | |
| Analysis of near-surface water[6] | Isotopic composition, tracers, bulk gas composition, and DIC | $CO_2$ dissolves in water. A meaningful analysis requires a thorough understanding of the geochemical cycle at the site. |
| Surface analysis of soil gas[7] | Composition of gas fluxes through the soil | $CO_2$ leaks would eventually percolate through the soil. Point measurements <1 $m^2$ are accurate but they lack spatial resolution |
| Near surface analysis of air composition[8] | $CO_2$ concentration in the near surface by infrared gas analyzer, eddy correlation tower, and light detection and ranging measure | $CO_2$ from leaks readily mix with other atmospheric gases. Local changes in turbulence and biological sources and sinks of $CO_2$ make the identification difficult. |
| *3. ON-SURFACE MONITORING* | | |
| Time-lapse 3D reflection seismic imaging[9] | P-wave velocity and amplitude | Takes advantage of low bulk modulus of $CO_2$. It is routinely used in the petroleum industry and can track the plume subsurface movement. |
| Gravity [10] | Mass density | $CO_2$ is generally lighter than water |
| Ground displacements[11] | Subsidence and heave, vertical displacement | $CO_2$ injection alters pore pressure and effect on effective stress, and therefore strata compressibility |
| Surface analysis of carbon content in soil[12] | Carbon content by Inelastic Neutron Scattering INS | Increased $CO_2$ levels asphyxiate aerobic organisms. |
| Remote sensing of air composition[7] | $CO_2$ atmospheric concentration by hyperspectral remote sensing of vegetative stress and long open path infrared absorption | Applicable at large scales |

(1) (Emberley *et al*., 2004; Gunter *et al*., 2000; Newell *et al*., 2008); (2) laboratory studies (Lei and Xue, 2009; Shi *et al*., 2007; Xue *et al*., 2005) and pilot tests (Bohnhoff *et al*., 2010; Daley *et al*., 2008; Daley *et al*., 2007; Onishi *et al*., 2009); (3) (Gasperikova and Hoversten, 2006; Nakatsuka *et al*., 2010); (4) (Bielinski *et al*., 2008); (5) (Charpentier *et al*., 2009); (6) (Oldenburg *et al*., 2003); (7) (Leuning *et al*., 2008; Oldenburg *et al*., 2003); (8) (Strazisar *et al*., 2009); (9) (Arts *et al*., 2004); (10) (Alnes *et al*., 2008); (11) (Alnes *et al*., 2008; Kempka *et al*., 2008); (12) (Wielopolski and Mitra, 2010)

$$\rho_{mix} = (1-n)\rho_s + n(S_{CO2}\rho_{CO2} + S_w\rho_w) \quad (12)$$

Then, the compressional $V_P$ and shear $V_S$ wave velocities are:

$$V_P = \sqrt{\left(\frac{B_{mix} + 4/3 \cdot G_{sk}}{\rho_{mix}}\right)} \quad (13)$$

$$V_S = \sqrt{\frac{G_{sk}}{\rho_{mix}}} \quad (14)$$

where $G_{sk}$ is the shear modulus of the mineral skeleton.

The electrical conductivity of a geological formation depends on the concentration and mobility of hydrated ions in the pore fluid and the volume fraction of fluid in the formation (Santamarina *et al*., 2001). The injection of $CO_2$ displaces the electrolyte (conductivity $\sigma_{fl}$) and the formation conductivity can be estimated using the Archie's equation (Mavko *et al*., 2009):

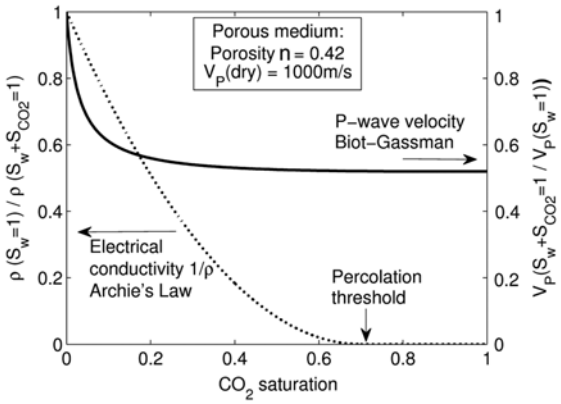


Fig. 10. Reduction of P-wave Velocity and Electrical Conductivity $\sigma_{form} = 1/\rho_{form}$ with $CO_2$ Saturation for a Sediment with Porosity $n$=0.42 (Ratio of P-wave velocity computed with $V_P$(Brine) = 1540 m/s, $V_P(CO_2)$ = 268 m/s (at $T$ = 40°C and P = 10 MPa), $V_P$(dry sediment) = 1000 m/s, and $\nu_{sk}$ = 0.1. electrical conductivity computed with an exponent $\beta$=2 for relative saturation and porosity, and a percolation threshold $S_{perc}$=0.7.)

$$\sigma_{form} = \sigma_{fl}[n(S_{perc}-S_{CO2})]^{\beta} \quad (15)$$

where $S_{CO2} \leq S_{perc}$, the maximum saturation of $CO_2$ at percolation. Figure 10 shows the variation of P-wave velocity $V_P$[m/s] and electrical conductivity $\sigma_{form}$ as a function of the $CO_2$ saturation $S_{CO2}$. Because $CO_2$ is non conductive and has a much lower bulk modulus than water, both $\sigma_{form}$ and $V_P$ decrease as the relative saturation $S_{CO2}$ increases. While forward predictions show a clear effect of $CO_2$ on $V_p$ and $\sigma_{form}$, the inverse analysis is hindered by measurement errors and error propagation. Hence, the estimation of $S_{CO2}$ from field measurements remains challenging.

## 5. Conclusions

- The volume of the geological formation that is affected by the injection of $CO_2$ depends on geometric boundaries, spatial variability, flow conditions and the emergence of viscous fingering.
- The physical properties of $CO_2$ such as density, viscosity, interfacial tension and bulk compressibility vary with pressure and temperature conditions, and must be properly modeled in numerical simulations of $CO_2$ geological storage.
- In particular, the $CO_2$-water interfacial tension decreases with fluid pressure. Lower interfacial tension reduces the capillary entry pressure for $CO_2$ into a water saturated seal cap rock.
- High $CO_2$ injection pressures can induce fluid driven fractures and trigger displacements along preexisting faults.
- The solubility of $CO_2$ in water is high as reservoir pressure conditions. The density of water increases with dissolved $CO_2$ and convective self-mixing takes place.
- Water acidification in the presence of $CO_2$ enhances mineral dissolution and alters the sediment fabric when clay minerals prevail. Silicates have a higher buffering capacity than calcite but the reaction rate is much slower.
- The evolution of dissolution and ensuing dissolution patterns depend on the interplay between the rates of advection, diffusion and dissolution. Dissolution may cause settlement, change in effective stress, and the formation of preferential channels for fluid flow, particularly in carbonates.
- The presence of $CO_2$ decreases the fluid bulk modulus, mass density, and electrical conductivity. These changes support the application of geophysical methods based on elastic and electromagnetic waves to monitor deep storage reservoirs. While forward predictions are manageable, inverse analysis is hindered by measurement difficulties and error propagation. Hence, the monitoring of $CO_2$ geological storage remains challenging.

## Acknowledgements

Support for this research was provided by the U. S. Department of Energy project DE-FE0001826 and the Goizueta Foundation. Any opinions, findings, conclusions, or recommendations expressed herein are those of the authors and do not necessarily reflect the views of funding organizations. C. Barrett carefully edited the original manuscript.

## References

Algive, L., Bekri, S., and Vizika-kavvadias, O. (2009). "Reactive pore network modeling dedicated to the determination of the petrophysical property changes while injecting $CO_2$." *SPE Annual Technical Conference and Exhibition, 4-7 October, New Orleans, Louisiana*, 124305-MS.

Alnes, H., Eiken, O., and Stenvold, T. (2008). "Monitoring gas production and $CO_2$ injection at the Sleipner field using time-lapse gravimetry." *Geophysics*, Vol. 73, No. 6, pp. WA155-WA161.

Armitage, P. J., Worden, R. H., Faulkner, D. R., Aplin, A. C., Butcher, A. R., and Iliffe, J. (2010). "Diagenetic and sedimentary controls on porosity in Lower Carboniferous fine-grained lithologies, Krechba field, Algeria: A petrological study of a caprock to a carbon capture site." *Marine and Petroleum Geology*, Vol. 27, No. 7, pp. 1395-1410.

Arts, R., Eiken, O., Chadwick, A., Zweigel, P., van der Meer, L., and Zinszner, B. (2004). "Monitoring of $CO_2$ injected at Sleipner using time-lapse seismic data." *Energy*, Vol. 29, Nos. 9-10, pp. 1383-1392.

Augustin, L., Barbante, C., Barnes, P., Barnola, J., Bigler, M., Castellano, E., Cattani, O., Chappellaz, J., Dahl-Jensen, D., and Delmonte, B. (2004). "Eight glacial cycles from an Antarctic ice core." *Nature*, Vol. 429, No. 6992, pp. 623-628.

Bielinski, A., Kopp, A., Schutt, H., and Class, H. (2008). "Monitoring of $CO_2$ plumes during storage in geological formations using temperature signals: Numerical investigation." *International Journal of Greenhouse Gas Control*, Vol. 2, No. 3, pp. 319-328.

Bjerrum, L., Kennard, R. M., Gibson, R. E., and Nash, J. (1972). "Hydraulic fracturing in field permeability testing." *Geotechnique*, Vol. 22, No. 2, pp. 319-332.

Blunt, M., Fayers, F. J., and Orr, F. M. (1993). "Carbon-dioxide in enhanced oil-recovery." *Energy Conversion and Management*, Vol.

34, Nos. 9-11, pp. 1197-1204.

Bohnhoff, M., Zoback, M. D., Chiaramonte, L., Gerst, J. L., and Gupta, N. (2010). "Seismic detection of $CO_2$ leakage along monitoring wellbores." *International Journal of Greenhouse Gas Control*, Vol. 4, No. 4, pp. 687-697.

Brown, M. A. and Southworth, F. (2008). "Mitigating climate change through green buildings and smart growth." *Environment and Planning A*, Vol. 40, No. 3, pp. 653-675.

CDIAC. (2009). *National $CO_2$ emissions from fossil-fuel burning, cement manufacture, and gas flaring: 1751-2007*, ORNL, http://cdiac.ornl.gov/ftp/ndp030/nation1751_2007.ems.

Ceglarska-Stefanska, G. and Zarebska, K. (2002a). "The competitive sorption of $CO_2$ and CH4 with regard to the release of methane from coal." *Fuel Processing Technology*, Vol. 77-78, pp. 423-429.

Ceglarska-Stefanska, G. and Zarebska, K. (2002b). "Expansion and contraction of variable rank coals during the exchange sorption of $CO_2$ and CH4." *Adsorption Science and Technology*, Vol. 20, No. 1, pp. 49-62.

Chalbaud, C., Robin, M., Lombard, J. M., Martin, F., Egermann, P., and Bertin, H. (2009). "Interfacial tension measurements and wettability evaluation for geological $CO_2$ storage." *Advances in Water Resources*, Vol. 32, No. 1, pp. 98-109.

Charpentier, F., Bureau, B., Troles, J., Boussard-Pledel, C., Michel-Le Pierres, K., Smektala, F., and Adam, J. L. (2009). "Infrared monitoring of underground $CO_2$ storage using chalcogenide glass fibers." *Optical Materials*, Vol. 31, No. 3, pp. 496-500.

Chi, S. M., Morsi, B. I., Klinzing, G. E., and Chiang, S. H. (1988). "Study of interfacial properties in the liquid $CO_2$ water coal system." *Energy & Fuels*, Vol. 2, No. 2, pp. 141-145.

Chiaramonte, L., Zoback, M., Friedmann, J., and Stamp, V. (2008). "Seal integrity and feasibility of $CO_2$ sequestration in the Teapot Dome EOR pilot: geomechanical site characterization." *Environmental Geology*, Vol. 54, No. 8, pp. 1667-1675.

Chiquet, P., Broseta, D., and Thibeau, S. (2007). "Wettability alteration of caprock minerals by carbon dioxide." *Geofluids*, Vol. 7, No. 2, pp. 112-122.

Daley, T. M., Myer, L. R., Peterson, J. E., Majer, E. L., and Hoversten, G. M. (2008). "Time-lapse crosswell seismic and VSP monitoring of injected $CO_2$ in a brine aquifer." *Environmental Geology*, Vol. 54, No. 8, pp. 1657-1665.

Daley, T. M., Solbau, R. D., Ajo-Franklin, J. B., and Benson, S. M. (2007). "Continuous active-source seismic monitoring of $CO_2$ injection in a brine aquifer." *Geophysics*, Vol. 72, No. 5, pp. A57-A61.

Delage, P., Cui, Y. J., and Schroeder, C. (1996). "Subsidence and capillary effects in chalks." *Dans EUROCK '96, Prediction and Performance in Rock Mechanics and Rock Engineering - ISRM International Symposium*, Torino : France.

Dickson, J. L., Gupta, G., Horozov, T. S., Binks, B. P., and Johnston, K. P. (2006). "Wetting phenomena at the $CO_2$/water/glass interface." *Langmuir,* Vol. 22, No. 5, pp. 2161-2170.

DOE. (2010). *Fossil fuels*, http://www.energy.gov/energysources/fossilfuels.htm, accessed on 11/14/2010.

DOE-NETL. (2008). *Carbon sequestration atlas of the United States of America and Canada*, Second Edition.

Dooley, J. J., Dahowski, R., Davidson, C., Wise, M. A., Gupta, N., Kim, S. H., and Malone, E. L. (2006). *Carbon dioxide capture and geologic storage: A core element of a global energy technology strategy to address climate change*, PNNL, Richland, WA.

Drever, J. I. (1997). *The geochemistry of natural waters: Surface and groundwater environments,* 3rd Ed., Prentice-Hall, New Jersey.

Duan, Z. and Sun, R. (2003). "An improved model calculating $CO_2$ solubility in pure water and aqueous NaCl solutions from 273 to 533 K and from 0 to 2000 bar." *Chemical Geology*, Vol. 193, Nos. 3-4, pp. 257-271.

Ehlig-Economides, C. and Economides, M. J. (2010). "Sequestering carbon dioxide in a closed underground volume." *Journal of Petroleum Science and Engineering*, Vol. 70, pp. 123-130.

Emberley, S., Hutcheon, I., Shevalier, M., Durocher, K., Gunter, W. D., and Perkins, E. H. (2004). "Geochemical monitoring of fluid-rock interaction and $CO_2$ storage at the Weyburn $CO_2$-injection enhanced oil recovery site, Saskatchewan, Canada." *Energy*, Vol. 29, Nos. 9-10, pp. 1393-1401.

Espinoza, D. N. and Santamarina, J. C. (2010). "Water-$CO_2$-mineral systems: Interfacial tension, contact angle and diffusion–Implications to $CO_2$ geological storage." *Water Resources Research*, Vol. 46(W07537), DOI:10.1029/2009WR008634.

Fenghour, A., Wakeham, W. A., and Vesovic, V. (1998). "The viscosity of carbon dioxide." *Journal of Physical and Chemical Reference Data*, Vol. 27, No. 1, pp. 31-44.

Fleury, M., Pironon, J., Le Nindre, Y. M., Bildstein, O., Berne, P., Lagneau, V., Broseta, D., Pichery, T., Fillacier, S., Lescanne, M., and Vidal, O. (2010). "Evaluating sealing efficiency of caprocks for $CO_2$ storage: An overview of the geocarbone-integrity program and results." *Oil & Gas Science and Technology-Revue De L Institut Francais Du Petrole*, Vol. 65, No. 3, pp. 435-444.

Forster, A., Norden, B., Zinck-Jorgensen, K., Frykman, P., Kulenkampff, J., Spangenberg, E., Erzinger, J., Zimmer, M., Kopp, J., and Borm, G. (2006). "Baseline characterization of the $CO_2$ SINK geological storage site at Ketzin, Germany." *Environmental Geosciences*, Vol. 13, No. 3, p. 145.

Fredd, C. and Fogler, H. (1998). "Influence of transport and reaction on wormhole formation in porous media." *AIChE Journal*, Vol. 44, No. 9, pp. 1933-1949.

Gale, J. (2004). "Geological storage of $CO_2$: What do we know, where are the gaps and what more needs to be done?." *Energy*, Vol. 29, Nos. 9-10, pp. 1329-1338.

Garcia, J. E. (2001). *Density of aqueous solutions of $CO_2$*, Lawrence Berkeley National Laboratory, http://escholarship.org/uc/item/6dn022hb.

Gasperikova, E. and Hoversten, G. M. (2006). "A feasibility study of nonseismic geophysical methods for monitoring geologic $CO_2$ sequestration." *The Leading Edge*(October), pp. 1282-1288.

Gaus, I., Azaroual, M., and Czernichowski-Lauriol, I. (2005). "Reactive transport modelling of the impact of $CO_2$ injection on the clayey cap rock at Sleipner (North Sea)." *Chemical Geology*, Vol. 217, Nos. 3-4, pp. 319-337.

Global-Carbon-Project. (2010). *The carbon budget 2009.*

Golfier, F., Zarcone, C., Bazin, B., Lenormand, R., Lasseux, D., and Quintard, M. (2002). "On the ability of a Darcy-scale model to capture wormhole formation during the dissolution of a porous medium." *Journal of fluid Mechanics*, Vol. 457, pp. 213-254.

Golomb, D. (1993). "Ocean disposal of $CO_2$ - feasibility, economics and effects." *Energy Conversion and Management*, Vol. 34, Nos. 9-11, pp. 967-976.

Gunter, W. D., Perkins, E. H., and Hutcheon, I. (2000). "Aquifer disposal of acid gases: Modelling of water-rock reactions for trapping of acid wastes." *Applied Geochemistry*, Vol. 15, No. 8, pp. 1085-1095.

Heddle, G., Herzog, H., and Klett, M. (2003). *The economics of $CO_2$*

*storage*, MIT LFEE, 2003-003 RP.

Hildenbrand, A., Schlomer, S., and Krooss, B. M. (2002). "Gas breakthrough experiments on fine-grained sedimentary rocks." *Geofluids*, Vol. 2, No. 1, pp. 3-23.

House, K. Z., Schrag, D. P., Harvey, C. F., and Lackner, K. S. (2006). "Permanent carbon dioxide storage in deep-sea sediments." *Proceedings of the National Academy of Sciences of the United States of America*, Vol. 103, No. 33, pp. 12291-12295.

IEA. (2009). *$CO_2$ emissions from fuel combustion highlights*.

IPCC. (2001). "Climate change 2001: The scientific basis. Contribution of working group I to the third assessment report of the intergovernmental panel on climate change. [Houghton, J. T., Y. Ding, D. J. Griggs, M. Noguer, P. J. van der Linden, X. Dai, K. Maskell, and C. A. Johnson (Eds.)]." IPCC, Ed., Cambridge University Press, United Kingdom and New York, p.881.

IPCC. (2005). *IPCC special report on carbon dioxide capture and storage. Prepared by working group III of the intergovernmental panel on climate change [Metz., B., O. Davidson, H. C. de Coninck, M. Loos, and L. A. Meyer (Eds.)]*, Cambridge University Press, Cambridge, United Kingdom and New York, NY, USA.

Israelachvili, J. (1991). *Intermolecular and surface forces,* 2nd Ed., Academic Press, London.

Jaccard, M. (2005). *Sustainable fossil fuels*, Cambridge University Press, New York, USA.

Jaky, J. (1944). "The coefficient of earth pressure at rest. In Hungarian (A nyugalmi nyomas tenyezoje)." *J. Soc. Hung. Eng. Arch. (Magyar Mernok es Epitesz-Egylet Kozlonye)*, pp. 355-358.

Jaworski, G. W., Duncan, J. M., and Seed, H. B. (1981). "Laboratory study of hydraulic fracturing." *J. Geotech. Eng. Div.*, Vol. 107, No. 6, pp. 713-732.

Kaszuba, J. P., Janecky, D. R., and Snow, M. G. (2005). "Experimental evaluation of mixed fluid reactions between supercritical carbon dioxide and NaCl brine: Relevance to the integrity of a geologic carbon repository." *Chemical Geology*, Vol. 217, Nos. 3-4, pp. 277-293.

Kempka, T., Waschbusch, M., Azzam, R., and Fernandez-Steeger, T. M. (2008). "Reducing ground subsidence involving geological $CO_2$ storage during longwall mining operations." *Quarterly Journal of Engineering Geology and Hydrogeology,* Vol. 41, pp. 439-448.

Kharaka, Y., Cole, D., Hovorka, S., Gunter, W., Knauss, K., and Freifeld, B. (2006). "Gas-water-rock interactions in Frio Formation following $CO_2$ injection: Implications for the storage of greenhouse gases in sedimentary basins." *Geology*, Vol. 34, No. 7, p.577.

Kiessling, D., Schmidt-Hattenberger, C., Schuett, H., Schilling, F., Krueger, K., Schoebel, B., Danckwardt, E., and Kummerow, J. (2010). "Geoelectrical methods for monitoring geological $CO_2$ storage: First results from cross-hole and surface-downhole measurements from the $CO_2$ SINK test site at Ketzin (Germany)." *International Journal of Greenhouse Gas Control*, Vol. 4, No. 5, pp. 816-826.

Kneafsey, T. J. and Pruess, K. (2010). "Laboratory flow experiments for visualizing carbon dioxide-induced, density-driven brine convection." *Transport in Porous Media*, Vol. 82, No. 1, pp. 123-139.

Kvamme, B., Kuznetsova, T., Hebach, A., Oberhof, A., and Lunde, E. (2007). "Measurements and modelling of interfacial tension for water plus carbon dioxide systems at elevated pressures." *Computational Materials Science*, Vol. 38, No. 3, pp. 506-513.

Larsen, J. W. (2004). "The effects of dissolved $CO_2$ on coal structure and properties." *International Journal of Coal Geology*, Vol. 57, No. 1, pp. 63-70.

Lei, X. L. and Xue, Z. Q. (2009). "Ultrasonic velocity and attenuation during $CO_2$ injection into water-saturated porous sandstone: Measurements using difference seismic tomography." *Physics of the Earth and Planetary Interiors*, Vol. 176, Nos. 3-4, pp. 224-234.

Lenormand, R., Touboul, E., and Zarcone, C. (1988). "Numerical-models and experiments on immiscible displacements in porous-media." *Journal of Fluid Mechanics,* Vol. 189, pp. 165-187. DOI:10.1017/S0022112088000953.

Leuning, R., Etheridge, D., Luhar, A., and Dunse, B. (2008). "Atmospheric monitoring and verification technologies for $CO_2$ geosequestration." *International Journal of Greenhouse Gas Control*, Vol. 2, No. 3, pp. 401-414.

Li, L., Peters, C., and Celia, M. (2006). "Upscaling geochemical reaction rates using pore-scale network modeling." *Advances in Water Resources*, Vol. 29, No. 9, pp. 1351-1370.

Mavko, G., Mukerji, T., and Dvorkin, J. (2009). *The rock physics handbook, second edition. Tools for seismic analysis of porous media*., Cambridge University Press, New York.

Mayne, P. W. and Kulhawy, F. H. (1982). "Ko-OCR Relationships in soil." *Journal of the Geotechnical Engineering Division-ASCE*, Vol. 108, No. 6, pp. 851-872.

Mazumder, S., Karnik, A., and Wolf, K. H. (2006). "Swelling of coal in response to $CO_2$ sequestration for ECBM and its effect on fracture permeability." *SPE Journal,* Vol. 11, Issue 3, pp. 390-398.

McGrail, B. P., Schaef, H. T., Glezakou, V.-A., Dang, L. X., and Owen, A. T. (2009). "Water reactivity in liquid and sc$CO_2$ phase: Has half the story been neglected?." *Energy Procedia GHGT-9*, Vol. 1, pp. 3415-3419.

Nakatsuka, Y., Xue, Z. Q., Garcia, H., and Matsuoka, T. (2010). "Experimental study on $CO_2$ monitoring and quantification of stored $CO_2$ in saline formations using resistivity measurements." *International Journal of Greenhouse Gas Control*, Vol. 4, No. 2, pp. 209-216.

National-Energy-Technology-Laboratory. (2010). *Carbon capture and storage database version* 2 <http://www.netl.doe.gov/technologies/carbon_seq/database>.

Newell, D. L., Kaszuba, J. P., Viswanathan, H. S., Pawar, R. J., and Carpenter, T. (2008). "Significance of carbonate buffers in natural waters reacting with supercritical $CO_2$: Implications for Monitoring, Measuring and Verification (MMV) of geologic carbon sequestration." *Geophysical Research Letters*, Vol. 35, L23403, DOI:10.1029/2008GL035615.

Obriot, J., Ge, J., Bose, T. K., and Starnaud, J. M. (1993). "Determination of the density from simultaneous measurements of the refractive-index and the dielectric-constant of gaseous CH4, SF6 and $CO_2$." *Fluid Phase Equilibria*, Vol. 86, pp. 315-350.

Oldenburg, C., Lewicki, J., and Hepple, R. (2003). *Near-surface monitoring strategies for geologic carbon dioxide storage verification*. Lawrence Berkeley National Laboratory Report LBNL-54089.

Onishi, K., Ueyama, T., Matsuoka, T., Nobuoka, D., Saito, H., Azuma, H., and Xue, Z. Q. (2009). "Application of crosswell seismic tomography using difference analysis with data normalization to monitor $CO_2$ flooding in an aquifer." *International Journal of Greenhouse Gas Control,* Vol. 3, No. 3, pp. 311-321.

Pacala, S. and Socolow, R. (2004). "Stabilization wedges: Solving the climate problem for the next 50 years with current technologies." *Science*, Vol. 305,No. 5686, pp. 968-972.

Pagnier, H. (2005). "Field experiment of ECBM-$CO_2$ in the upper silesian basin of Poland (RECOPOL)." *SPE Europec/EAGE Annual*

*Conference*, Madrid, Spain.

Palomino, A. M. and Santamarina, J. C. (2005). "Fabric map for kaolinite: Effects of pH and ionic concentration on behavior." *Clays and Clay Minerals*, Vol. 53, No. 3, pp. 211-223.

Pekot, J. L. and Reeves, S. R. (2002). *Modeling coal matrix shrinkage and differential swelling with $CO_2$ injection for enhanced coalbed methane recovery and carbon sequestration applications*, Advanced Resources International - U.S. Department of Energy, Houston, Texas.

Peng, D. and Robinson, D. B. (1976). "New 2-constant equation of state." *Industrial & Engineering Chemistry Fundamentals*, Vol. 15, No. 1, pp. 59-64.

Pennell, K. D., Pope, G. A., and Abriola, L. M. (1996). "Influence of viscous and buoyancy forces on the mobilization of residual tetrachloroethylene during surfactant flushing." *Environmental Science & Technology*, Vol. 30, No. 4, pp. 1328-1335.

Pokrovsky, O., Golubev, S., and Schott, J. (2005). "Dissolution kinetics of calcite, dolomite and magnesite at 25 C and 0 to 50 atm $pCO_2$." *Chemical Geology*, Vol. 217, Nos. 3-4, pp. 239-255.

Pusch, G., Ionescu, G. F., May, F., Voigtlander, G., Stecken, L., and Vosteen, H. D. (2010). "Common features of carbon dioxide and underground gas storage (1)." *Oil Gas-European Magazine*, Vol. 36, No. 3, pp. 131-137.

Renard, F., Gundersen, E., Hellmann, R., Collombet, M., and Le-Guen, Y. (2005). "Numerical modeling of the effect of carbon dioxide sequestration on the rate of pressure solution creep in limestone: Preliminary results." *Oil & Gas Science and Technology – Rev. IFP*, Vol. 60, No. 2, pp. 381-399.

Riaz, A., Hesse, M., Tchelepi, H. A., and Orr, F. M. (2006). "Onset of convection in a gravitationally unstable diffusive boundary layer in porous media." *Journal of Fluid Mechanics,* Vol. 548, pp. 87-111.

Rutqvist, J. and Tsang, C. (2002). "A study of caprock hydromechanical changes associated with $CO_2$-injection into a brine formation." *Environmental Geology*, Vol. 42, No. 2, pp. 296-305.

Rutqvist, J., Vasco, D., and Myer, L. (2009). "Coupled reservoir-geomechanical analysis of $CO_2$ injection at In Salah, Algeria." *Energy Procedia*, Vol. 1, No. 1, pp. 1847-1854.

Santamarina, J. C., Klein, K. A., and Fam, M. A. (2001). *Soils and waves*, Wiley.

Shi, J., Durucan, S., and Fujioka, M. (2008). "A reservoir simulation study of $CO_2$ injection and N2 flooding at the Ishikari coalfield $CO_2$ storage pilot project, Japan." *International Journal of Greenhouse Gas Control*, Vol. 2, No. 1, pp. 47-57.

Shi, J. Q., Xue, Z. Q., and Durucan, S. (2007). "Seismic monitoring and modelling of supercritical $CO_2$ injection into a water-saturated sandstone: Interpretation of P-wave velocity data." *International Journal of Greenhouse Gas Control*, Vol. 1, No. 4, pp. 473-480.

Shin, H. and Santamarina, J. (2009). "Mineral dissolution and the evolution of k0." *Journal of Geotechnical and Geoenvironmental Engineering*, Vol. 135, p.1141.

Shin, H. and Santamarina, J. C. (2010). "Fluid-driven fractures in uncemented sediments: Underlying particle-level processes." *Earth and Planetary Science Letters*, Vol. 299, No. 1-2, pp. 180-189.

Shin, H., Santamarina, J. C., and Cartwright, J. A. (2008). "Contraction-driven shear failure in compacting uncemented sediments." *Geology*, Vol. 36, No. 12, pp. 931-934.

Sloan, E. D. and Koh, C. A. (2008). *Clathrate hydrates of natural gases, 3rd Ed.*, CRC Press, Boca Raton, FL.

Solomon, S. (2007). *Climate change 2007: The physical science basis: Contribution of working group i to the fourth assessment report of the intergovernmental panel on climate change*, Cambridge University Press.

Somerton, W. H., Soylemezolu, I. M., and Dudley, R. C. (1975). "Effect of stress on permeability of coal." *International Journal of Rock Mechanics and Mining Science & Geomechanics Abstracts*, Vol. 12, Nos. 5-6, pp. 129-145.

Span, R. and Wagner, W. (1996). "A new equation of state for carbon dioxide covering the fluid region from the triple-point temperature to 1100 K at pressures up to 800 MPa." *Journal of Physical and Chemical Reference Data*, Vol. 25, No. 6, pp. 1509-1596.

Spycher, N., Pruess, K., and Ennis-King, J. (2003). "$CO_2$-H2O mixtures in the geological sequestration of $CO_2$. I. Assessment and calculation of mutual solubilities from 12 to 100 degrees C and up to 600 bar." *Geochimica Et Cosmochimica Acta*, Vol. 67, No. 16, pp. 3015-3031.

Strazisar, B. R., Wells, A. W., Diehl, J. R., Hammack, R. W., and Veloski, G. A. (2009). "Near-surface monitoring for the ZERT shallow $CO_2$ injection project." *International Journal of Greenhouse Gas Control*, Vol. 3, No. 6, pp. 736-744.

Streit, E. E. and Hillis, R. R. (2004). "Estimating fault stability and sustainable fluid pressures for underground storage of $CO_2$ in porous rock." *Energy,* Vol. 29, Nos. 9-10, pp. 1445-1456.

Stumm, W. and Morgan, J. J. (1996). *Aquatic chemistry: Chemical equilibria and rates in natural waters,* 3rd Ed., JohnWiley & Sons, Inc, New York.

Takenouchi, S. and Kennedy, G. (1965). "Dissociation pressures of the phase $CO_2 \cdot 5.75$ H2O." *J. Geol*, Vol. 73, pp. 383-390.

Verdon, J. and Woods, A. (2007). "Gravity-driven reacting flows in a confined porous aquifer." *Journal of fluid Mechanics*, Vol. 588, pp. 29-41.

Watson, M. N., Zwingmann, N., and Lemon, N. M. (2004). "The ladbroke grove-katnook carbon dioxide natural laboratory: A recent $CO_2$ accumulation in a lithic sandstone reservoir." *Energy*, Vol. 29, Nos. 9-10, pp. 1457-1466.

White, D., Burrowes, G., Davis, T., Hajnal, Z., Hirsche, I., Hutcheon, K., Majer, E., Rostron, B., and Whittaker, S. (2004). "Greenhouse gas sequestration in abandoned oil reservoirs." *The International Energy Agency Weyburn pilot project. GSA Today*, Vol. 14, pp. 4-10.

Wielopolski, L. and Mitra, S. (2010). "Near-surface soil carbon detection for monitoring $CO_2$ seepage from a geological reservoir." *Environmental Earth Sciences*, Vol. 60, No. 2, pp. 307-312.

World-Resources-Institute. (2010a). *Climate analysis indicator tool (CAIT) version 7.0*.

World-Resources-Institute. (2010b). *Earth trends (energy and resources - country profiles)* <http://earthtrends.wri.org>.

Xue, Z. Q., Ohsumi, T., and Koide, H. (2005). "An experimental study on seismic monitoring of a $CO_2$ flooding in two sandstones." *Energy*, Vol. 30, Nos. 11-12, pp. 2352-2359.

Zhai, Z. and Sharma, M. M. (2005). "A new approach to modeling hydraulic fractures in unconsolidated sands." *SPE Annual Technical Conference and Exhibition*.